AGU PUBLICATIONS

Geophysical Research Letters

RESEARCH LETTER
10.1002/2017GL072931

Key Points:
- Decadal variability of O_2 and subsurface tracers in CCS primarily driven by physical processes
- Subsurface anomalies from the gyre propagate downstream into the CCS through mean circulation
- Subsurface ocean decadal variability may be exploited for predicting tracers in upwelling systems

Supporting Information:
- Supporting Information S1

Correspondence to:
M. Pozo Buil,
mercedes.pozo@eas.gatech.edu

Citation:
Pozo Buil, M., and E. Di Lorenzo (2017), Decadal dynamics and predictability of oxygen and subsurface tracers in the California Current System, *Geophys. Res. Lett.*, *44*, doi:10.1002/2017GL072931.

Received 2 FEB 2017
Accepted 7 APR 2017
Accepted article online 12 APR 2017

Decadal dynamics and predictability of oxygen and subsurface tracers in the California Current System

Mercedes Pozo Buil[1] and **Emanuele Di Lorenzo**[1]

[1]School of Earth and Atmospheric Sciences, Georgia Institute of Technology, Atlanta, Georgia, USA

Abstract The oxygen of the source waters that feed the upwelling in the California Current System shows prominent multidecadal fluctuations that are not significantly correlated with the dominant modes of Pacific climate variability. By combining observations and ocean reanalysis products between 1950 and 2010, we show that decadal changes in oxygen are linked to subsurface salinity variability and primarily controlled by ocean circulation dynamics. We find that subsurface anomalies in the core of the North Pacific Current propagate the oxygen signal downstream into the coastal upwelling system following the path of the mean gyre circulation with a time scale of 10 years. These results suggest that decadal variability in the ocean subsurface is a key process for understanding, and potentially predicting, hypoxia and other biogeochemical tracers in upwelling systems. According to the current sign of the subsurface tracer anomalies in the gyre, California may experience a new period of strong decline in oxygen by 2020.

1. Introduction

Coastal ocean hypoxia has emerged as a growing threat to marine ecosystems and fisheries and raises concerns for human health [*Diaz and Rosenberg*, 2008; *McClatchie et al.*, 2010; *Rabalais et al.*, 2010]. In the California Current System (CCS), like most other coastal ocean upwelling systems, changes in the oxygen content are controlled by complex interactions between circulation and biogeochemistry and show prominent fluctuations on interannual and decadal time scales [*Bograd et al.*, 2008; *Crawford and Pena*, 2016; *Deutsch et al.*, 2006, 2011].

Over the shelf region where the marine ecosystem is most sensitive to hypoxia, changes in oxygen are strongly controlled by coastal upwelling [*Bograd et al.*, 2008; *Chan et al.*, 2008; *Connolly et al.*, 2010]. Vertical fluxes of nutrient-rich subsurface waters to the surface can trigger high production of new organic matter on the shelf. As the organic matter sinks, bacterial decomposition in the subsurface depletes oxygen leading to hypoxic events [*Chan et al.*, 2008; *Grantham et al.*, 2004].

While wind-induced upwelling and biological processes drive the interannual variability of the oxygen content on the shelf [*Checkley and Barth*, 2009; *Connolly et al.*, 2010; *Peterson et al.*, 2013], it has been recognized that long-term changes in the oxygen content of the CCS source waters for the coastal upwelling are equally important [*Bograd et al.*, 2015] and may influence the statistics of coastal hypoxia. This latter process is summarized in the idealized cross-shore vertical model of coastal upwelling in schematic Figure 1. This model illustrates how the pool of subsurface water masses (the green shadow region) contributes to the oxygen content in the shelf (the red shadow region) through mean upwelling (gray arrows).

Below the mixed layer, oxygen anomalies on the shelf of the southern CCS have undergone a large decline (approximately a 20%) over the last three decades [*Bograd et al.*, 2008] (from 1980 to 2012; Figure 2a, red line). Similar declining oxygen values have been reported over the continental shelf of the northern CCS [*Peterson et al.*, 2013] (from 1998 to 2012; Figure 2a, orange line). *Meinvielle and Johnson* [2013] find similar declining trends all along the continental shelf break between 25° and 50°N with a maximum near the core of the California Undercurrent (CUC). While these drops in oxygen values exhibit the longest and the strongest negative trend in the observed oxygen time series over the CCS, an extension of the time series to 1950 in the southern CCS [*Koslow et al.*, 2011] (Figure 2a, red line) and to 1960 in the northern CCS [*Pierce et al.*, 2012] (Figure 2a, orange line) shows that this trend is neither monotonic [*McClatchie et al.*, 2010] nor significant [*Koslow et al.*, 2011]. Therefore, the observed oxygen variability is best characterized in terms of multidecadal fluctuations rather than a negative trend [*Bograd et al.*, 2008; *Meinvielle and Johnson*, 2013; *Pierce et al.*, 2012; *Whitney et al.*, 2007]. Additional analysis of the CCS oxygen data [*Deutsch et al.*, 2011] (Figure 2a, green line) confirms that the variability of oxygen anomalies in the CCS is strongly modulated by a multidecadal

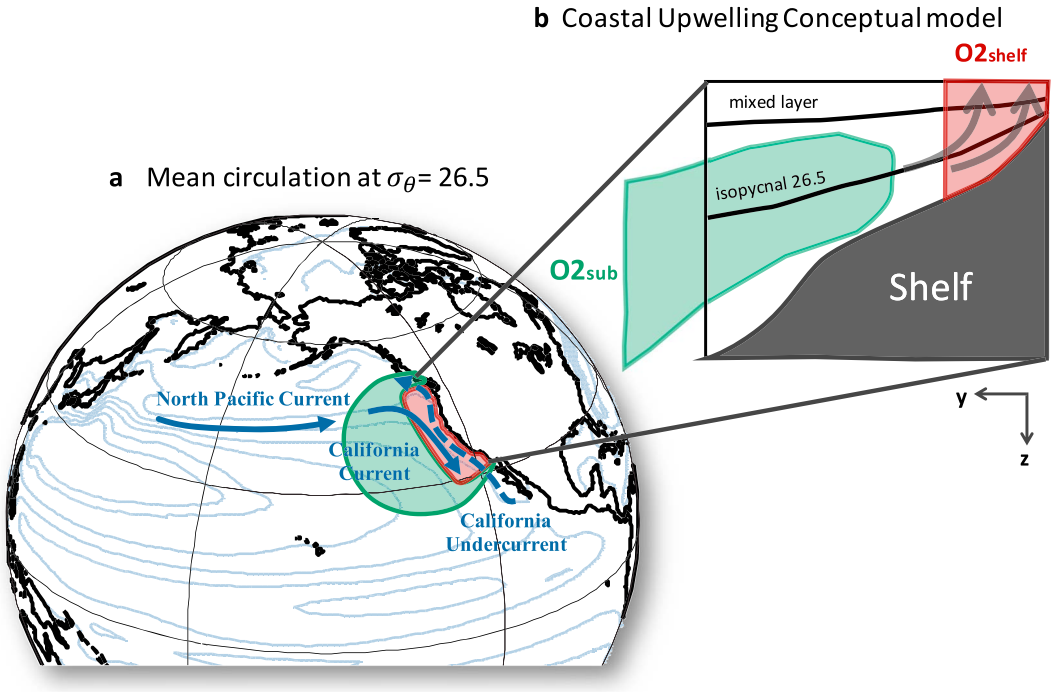

Figure 1. Conceptual model of water masses upwelling in the CCS. (a) Contours represent the ORA-S3 mean Bernoulli's stream function along isopycnal 26.5 from 1959 to 2010 showing the path of the mean subsurface circulation. The blue arrows represent the major currents that converge in the CCS region: North Pacific Current, California Current, and California Undercurrent. (b) Idealized cross-shore vertical profile of the shelf to illustrate large-scale subsurface dynamics impacting oxygen in shelf coastal waters. The pool of subsurface waters (green shadow region) feed the main upwelling (gray arrows) and impact the control volume of oxygen content in the shelf (red shadow region).

oscillation [*Deutsch et al.*, 2011]. This type of decadal variability is also reported in a recent study [*Crawford and Pena*, 2016] showing a significant dome-shaped temporal pattern of subsurface oxygen in the California Cooperative Oceanic Fisheries Investigations (CalCOFI) region. In the subsurface, tracers like oxygen, salinity, and temperature are expected to have a predominant multidecadal time scale because of the long-term memory of the ocean and of "double-integration" effects [*Di Lorenzo and Ohman*, 2013; *Ito and Deutsch*, 2010; *Kilpatrick et al.*, 2011]. In the subsurface, ocean tracers integrate the variability associated with geostrophic currents, which are already the result of an integration of the surface atmospheric forcing. These double-integration effects lead to a very strong reddening (i.e., amplification of low-frequency variance) of the tracers' spectrum.

Previous studies have explored the role of large-scale climate processes such as the Pacific Decadal Oscillation (PDO) and North Pacific Gyre Oscillation (NPGO) [*Deutsch et al.*, 2011; *Di Lorenzo et al.*, 2008; *Peterson et al.*, 2013] as generating mechanisms for the low-frequency fluctuations of oxygen in the CCS. While climate modes like PDO and NPGO share correlation with the full-length oxygen CalCOFI time series of *Koslow et al.* [2011] with values of $R \sim 0.4$, this correlation is higher in the summer when the climate modes are weak and is not statistically significant if we account for the large autocorrelation in the oxygen data. Given that PDO and NPGO are defined by using sea surface temperature [*Mantua et al.*, 1997] and height [*Di Lorenzo et al.*, 2008], the modes capture variability confined in the upper ocean (e.g., 0–150 m) [*Chhak et al.*, 2009] and are not necessarily good indicators of the oxygen subsurface dynamics.

In the thermocline, large-scale horizontal circulation plays an important role in modulating the variability of subsurface water properties in the eastern North Pacific [*Chikamoto et al.*, 2015; *Kilpatrick et al.*, 2011], Gulf of Alaska [*Pozo Buil and Di Lorenzo*, 2015], and CCS [*Bograd et al.*, 2015; *Peterson et al.*, 2013]. Zonal subsurface advection from the North Pacific gyre into the CCS draws young water masses characterized by high oxygen (Figure 2c) and low nutrient concentration [*Hickey*, 1979; *Lynn and Simpson*, 1987]. These source waters also transport the low-salinity signature from ventilated thermocline waters (Figure 2d) in the western Pacific [*Hickey*, 1979]. From the south, the California Undercurrent (CUC)

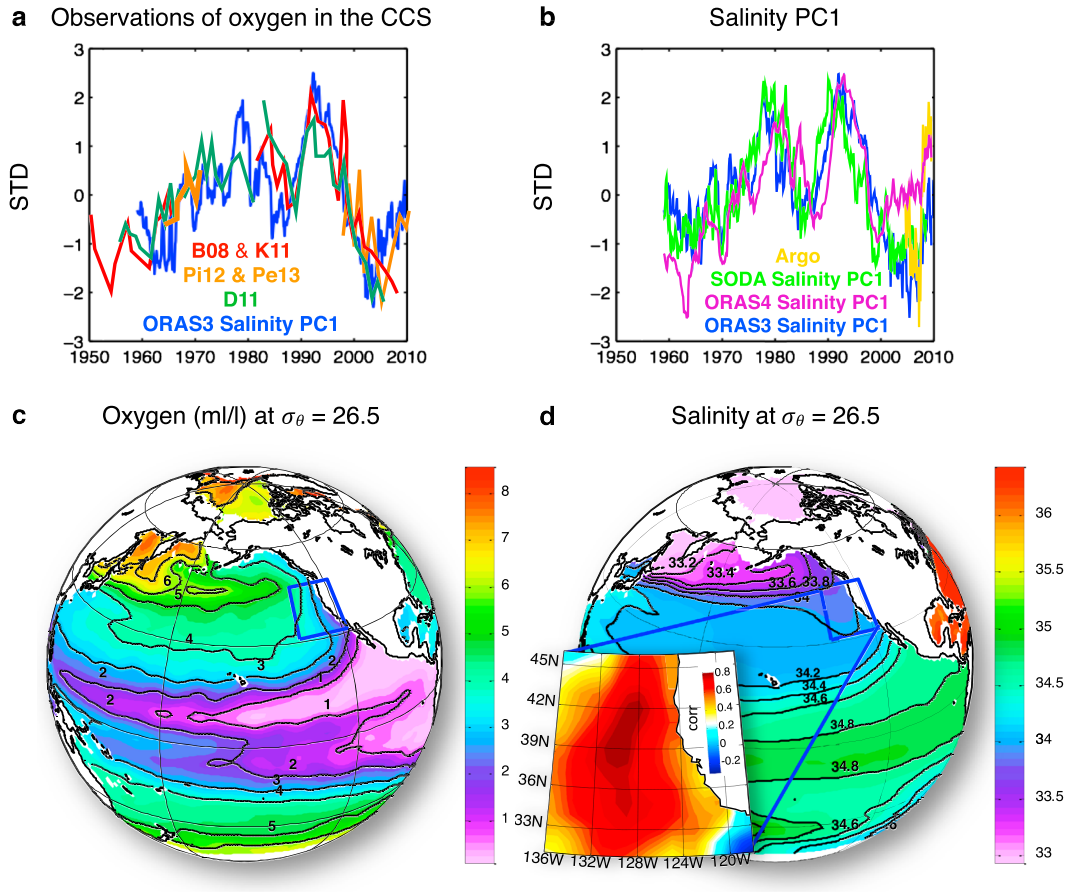

Figure 2. Low-frequency variability of the subsurface oxygen content (oxygen content on the 26.5 kg m^{-3} isopycnal surface) in the CCS. (a) Time series of the observed oxygen along the West Coast of North America: *Bograd et al.* [2008] and *Koslow et al.* [2011] (B08 and K11; red line), *Pierce et al.* [2012] and *Peterson et al.* [2013] (Pi12 and Pe13; orange line), *Deutsch et al.* [2011] (D11; green line), and ORA-S3 salinity leading pattern or principal component (PC1; blue line). (b) Time series of the PC1 of salinity for ORA-S3 (blue line, same as in Figure 1a), ORA-S4 (purple line), SODA 2.1.6 (green line), and Argo mean salinity anomalies (yellow line) on the region of the PC1 (blue square in Figure 1d). (c) Annual mean dissolved oxygen distribution (mL/L) and (d) salinity (psu) along the isopycnal 26.5 kg m^{-3} on the Pacific Ocean from the World Ocean Database 2013 [*Boyer et al.*, 2013]. The ORA-S3 salinity PC1 (blue line) is computed from normalized salinity anomalies on the isopycnal 26.5 in the region of the blue box in Figures 1c and 1d. The spatial pattern of the salinity PC1 is shown as a pop-up of the CCS region. The units for the colorbar of the pop-up are correlations between PC1 and salinity anomalies on the isopycnal 26.5.

transports along the upper continental slope old, salty, and oxygen-depleted waters from the tropical oxygen minimum zones [*Gay and Chereskin*, 2009; *Lynn and Simpson*, 1987; *Wyrtki*, 1962] (Figures 2c and 2d), where the weak ocean ventilation and biogeochemical transformations maintain low oxygen levels [*Bograd et al.*, 2008; *Hickey*, 1979; *Stramma et al.*, 2010], to all the way to Alaska [*Thomson and Krassovski*, 2010].

In this study, we hypothesize that decadal changes in the oxygen content of the CCS upwelling source waters are primarily controlled by the transport of subsurface water mass anomalies associated with the mean gyre-scale circulation (i.e., mean advection of subsurface water mass anomalies). Diagnosing the decadal dynamics of subsurface oxygen is complicated given the lack of spatially and temporally resolved oxygen observations. However, to the extent that biological controls play a minor role in the multidecadal variability of subsurface oxygen [e.g., *Deutsch et al.*, 2006], changes in oxygen should be correlated with physical tracers like salinity and temperature on isopycnal layers, which are better sampled spatially and temporally. The goal of this paper is to show that long-term oxygen variability recorded in the California Current System has a predominant subsurface physical control associated with the decadal propagation of water mass anomalies transported by the gyre-scale circulation, which is inherently predictable.

The remainder of the paper is organized as follows. Section 2 describes the data and the methodology used in this study. Section 3 introduces a salinity-based physical proxy for subsurface oxygen and its validation with observational long-term data along the CCS. Section 4 uses the salinity-based physical proxy to investigate the physical controls of multidecadal oxygen variability. A summary and discussion of the implications for decadal predictability of oxygen of the CCS upwelling source waters are provided in section 5.

2. Data and Methods

The reference time series for the observed multidecadal variability of oxygen in the CCS (Figure 2a) are taken from previous published work [*Bograd et al.*, 2008; *Deutsch et al.*, 2011; *Koslow et al.*, 2011; *Peterson et al.*, 2013; *Pierce et al.*, 2012] and cover the period of 1950–2010. These time series are developed by using different analyses of subsurface oxygen from the CalCOFI hydropgrahy [*Bograd et al.*, 2008; *Deutsch et al.*, 2011; *Koslow et al.*, 2011] and data collected in the Oregon Shelf [*Peterson et al.*, 2013; *Pierce et al.*, 2012]. For the purpose of computing correlations with the CCS oxygen time series we use the CalCOFI portion of the data updated by Koslow and Bograd (personal communication), which has more temporal coverage.

To explore the physical control of subsurface oxygen, we focus our analysis on the $\sigma_\theta = 26.5$ kg m^{-3} isopycnal surface, which ventilates in the western subarctic Pacific and does not outcrop in CCS during winter. To perform the isopycnal analysis, we use primarily salinity and temperature data from the European Centre for Medium-Range Weather Forecasts (ECMWF) Ocean Reanalysis System (ORA-S3) [*Balmaseda et al.*, 2008] over the period of 1959–2009. Results obtained from the ORA-S3 analysis are also compared to the Simple Ocean Data Assimilation (SODA; version 2.1.6) [*Carton and Giese*, 2008], the ECMWF ORA-S4 [*Balmaseda et al.*, 2013], and available gridded Argo observations. Using the monthly temperature and salinity fields, we calculate the potential density field for each vertical level according to the United Nations Educational, Scientific and Cultural Organization International Equation of State [*UNESCO*, 1983]. Then fields are linearly interpolated onto isopycnal surfaces by using the transformation from z coordinates to sigma-coordinate system method [*Chu et al.*, 2002]. We use the same approach for all reanalysis and Argo products.

To define the mean gyre-scale circulation along the 26.5 kg m^{-3} isopycnal surface, we compute the Bernoulli stream function assuming constant density along streamlines and then integrating the pressure of a column of water above each point on the isopycnal layer.

Here we estimate the significance of the correlation coefficients (R) between two time series by using a Monte Carlo method. In this approach, each time series is approximated as a first-order autoregressive (AR-1) model with the same autoregression coefficient computed from the original time series. We use the AR-1 models to simulate 5000 realizations of two random red-noise time series. The final percent significance is then determined based on the probability distribution function of the cross-correlation coefficients between the two time series.

3. Physical Controls of Multidecadal Oxygen Variability

To test the extent to which multidecadal variability in the oxygen source waters of the CCS upwelling is primarily controlled by changes in the physical dynamics, we compare the available observed oxygen time series to the variability of a subsurface passive tracer such as salinity on a constant density surface ($\sigma_\theta = 26.5$ kg m^{-3}) located below the ocean mixed layer. The choice of salinity is motivated by the high spatial correlation of the annual mean salinity and dissolved oxygen concentration in the North Pacific (high salinity ➔ low oxygen; Figures 2c and 2d). To characterize the subsurface physical variability, we extract the leading empirical orthogonal function (EOF1) of the salinity anomalies on the isopycnal 26.5 in the CCS region defined by coordinates 136°W–118°W and 31°N–46.5°N (Figure 2d, blue square). The time series of this leading pattern or principal component (PC1; Figure 2a, blue line) inferred from ECMWF ORA-S3 is compared to the available oxygen observations (Figure 2a) and with other observational products and reanalysis (Figure 2b). We find a strong correlation (R = 0.71, >99% significance level) between the salinity PC1 and the CalCOFI oxygen time series (Figure 2a). When comparing the PC1 from ORA-S3 to the SODA and ORA-S4 reanalysis, we find overall good agreement with correlations R = 0.8 and R = 0.75. The Argo data are also in agreement with the ORA-S3, but the timespan of the data is too short for any meaningful

correlations. The ORA-S4 shows an anomalous higher salinity between 2000 and 2010 that is not evident in all the other data sets, including Argo and the CalCOFI oxygen data.

The alignment between the ORA-S3 salinity proxy (salinity PC1) and the observational oxygen data supports our hypothesis that the multidecadal variability of the oxygen content is primarily controlled by ocean subsurface circulation dynamics, rather than biological and chemical processes. Additional support for this hypothesis is evident from the strong correlation (R = 0.71, >99% significance level) that exists between the CalCOFI oxygen time series and the saturation (solubility) of oxygen inferred from ECMWF ORA-S3 subsurface temperature and salinity fields (following equation 8 from *Garcia and Gordon* [1992]), which is expected since temperature and salinity are compensated on a given isopycnal surface [*Veronis*, 1972]. To further explore the consistency of the ORA-S3 reanalysis in capturing subsurface signals, we compare a time series of subsurface salinity anomalies from the ORA-S3 data set with available long-term salinity and oxygen observations (data courtesy of W. Crawford) at Ocean Station P (OSP) (Figure S1 in the supporting information), located in the subpolar gyre (50°N, 145°W). Although OSP is outside the CCS domain, the high and significant correlation between OSP observations and ORA-S3 (R = 0.63 for salinity and R = 0.38 for oxygen) confirms that the ORA-S3 accurately captures the large-scale dynamics of subsurface salinity and oxygen in Northeast Pacific region. This enables us to use salinity anomalies on the isopycnal 26.5 as a proxy for exploring the multidecadal dynamics of subsurface oxygen variability along the Pacific eastern boundary upwelling system.

4. Decadal Dynamics of Subsurface Tracers and Oxygen

We hypothesize that multidecadal changes in subsurface tracers (e.g., salinity and temperature) and oxygen (e.g., σ_θ = 26.5 kg m^{-3}) in the CCS are controlled by anomalies that propagate along the path of the mean gyre circulation. To test this hypothesis, we explore the subsurface propagation dynamics of salinity anomalies, which we have identified as a close proxy for decadal changes of oxygen. We define an index of normalized salinity anomalies on σ_θ = 26.5 kg m^{-3} along the coasts of Washington, Oregon, and California, that is the region of the CCS upwelling source waters and where the North Pacific Current reaches the eastern coastal boundary (Figure 3e, red box, shows the region used to average the salinity; Figure 3h, red line, shows the coastal salinity index). We then compute lead/lag correlation maps between this coastal salinity index and the salinity on the entire isopycnal surface over the eastern and central North Pacific (Figures 3a–3f). At zero lag (Figure 3e), the correlation pattern shows a broad region extending from the coast to the offshore for about 1000 km. This pattern decays at the coast at a 3 year lag (Figure 3f). In the growth phase at 3 year lead (Figure 3d), the correlation pattern shows that the center of action has shifted offshore along the axis of the southward branch of the subtropical gyre. The 3 year lead pattern is almost identical to the EOF1/PC1 of salinity in the CCS region (compare Figure 3d with Figure 2d), which we use as our proxy for the observed multidecadal variability of oxygen in the CCS. We verify that by comparing PC1 to the coastal salinity index with a lead of 3 year, which show significant correlation (R = 0.77; Figure 3h). Further inspection of the spatial and temporal progression of the correlation maps at leads 6, 9, and 12 years (Figures 3a–3c) shows a clear backward propagation of the salinity anomalies along the path of the mean gyre suggesting that multidecadal variability of salinity and oxygen in the CCS region is controlled by advection of anomalies along the mean circulation. In fact, at lead 12 years (Figure 3a), we find significant correlations along the axis of the North Pacific Current in excess of 0.65. These lead times are consistent with the mean advection time scales in the eastern North Pacific estimated using the ORA-S3 reanalysis data set (Figure S2). To further visualize the connection between the gyre anomalies, salinity PC1 (e.g., proxy for oxygen), and the coastal salinity, we compare an index of gyre salinity anomalies (e.g., the average salinity anomaly in the green box of Figure 3a) with the salinity PC1 (Figure 3g) and the coastal salinity index (Figure 3i) with the appropriate lags of 9 and 12 years later. The time series exhibit strong and significant correlation R = 0.59 (gyre salinity versus PC1) and R = 0.66 (gyre salinity versus coastal salinity) with a dominant multidecadal signal. These propagation dynamics are consistent with other reanalysis products (e.g., ORA-S4 and SODA; Figure 4). While ORA-S4 replicates the propagation pattern of the salinity anomalies found in ORA-S3 (compare Figures 3a–3e to Figure 4a), with a slight expansion of the correlation signal at lead 12 years, SODA shows a general weakening and loss of significance of the propagation pattern (compare Figures 3a–3e to Figure 4b). These differences may arise from the differences in the models and assimilations methods used to generate the reanalysis products [*Balmaseda et al.*, 2008, 2013; *Carton and Giese*, 2008]. For example, the assimilation scheme used in SODA does not preserve the integrity of subsurface water masses on isopycnals.

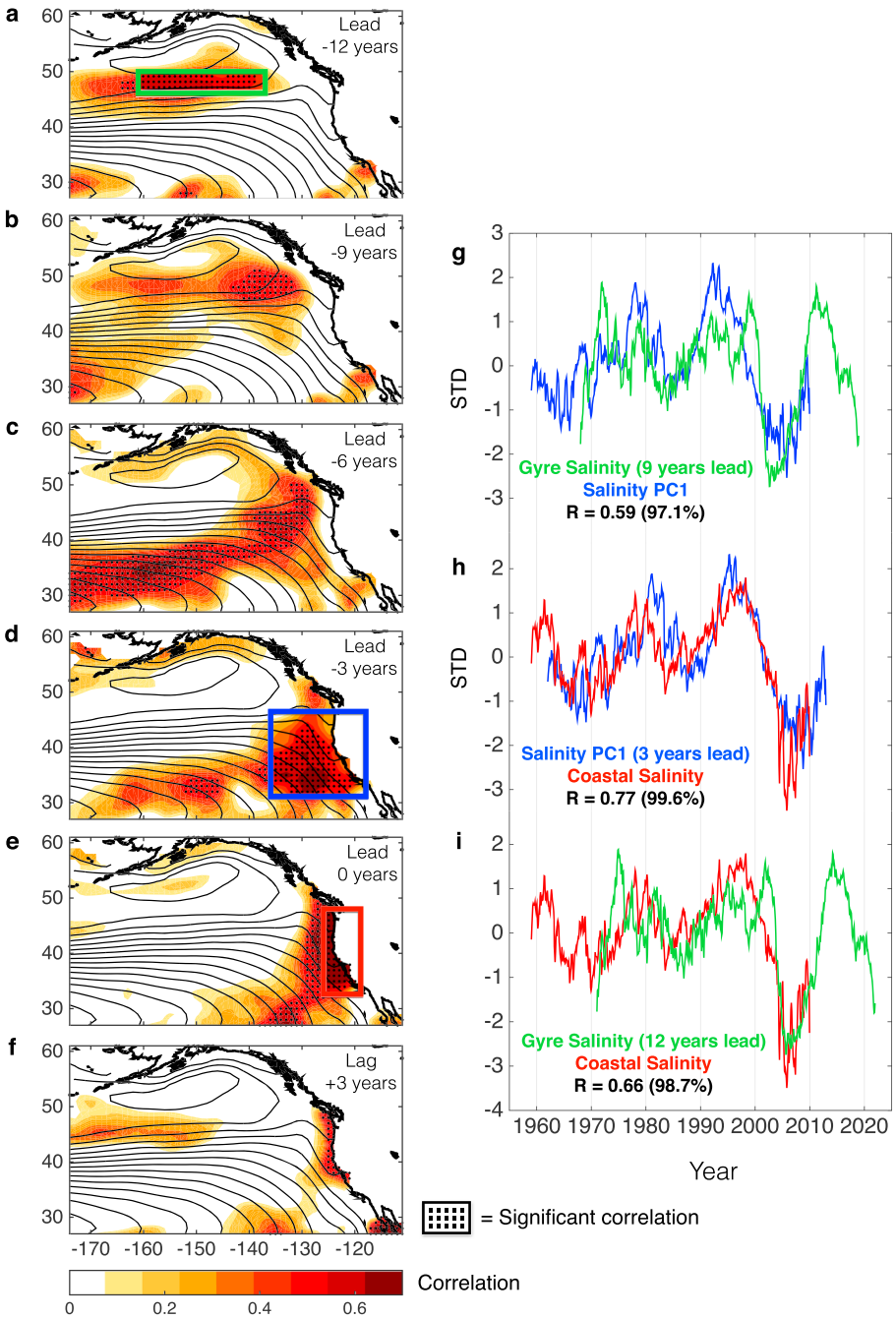

Figure 3. Subsurface propagation of salinity anomalies. (a–f) Lead/lag correlation maps between the salinity anomalies on the $\sigma_\theta = 26.5$ kg m^{-3} isopycnal surface and the coastal salinity index from lead 12 years (Figure 3a) to lag 3 years (Figure 3f), in increments of 3 years. Only positive correlations are plotted in the shading. The contours represent the mean Bernoulli's stream function along isopycnal 26.5 showing the path of the mean subsurface circulation. The coastal salinity index (red line in Figures 3h and 3i) is the average salinity anomaly on the $\sigma_\theta = 26.5$ kg m^{-3} isopycnal in the region of the red box (coordinates 126°W–119°W and 32.5°N–48°N). The salinity PC1 (blue line in Figures 3g and 3h is the time series of leading mode of the salinity defined in the blue box (Figure 3d). The salinity gyre index (green line, Figures 3g and 3i) is defined as the spatially average salinity anomaly upstream the gyre in the region of the green box (coordinates 161°W–137°W and 46°N–50°N). The salinity gyre index leads the salinity PC1 and the coastal salinity index by 9 (Figure 3g) and 12 years (Figure 3i), respectively. The salinity PC1 leads the coastal index by 3 years (Figure 3h). All the figures have been done by using the ECMWF ORA-S3 data set.

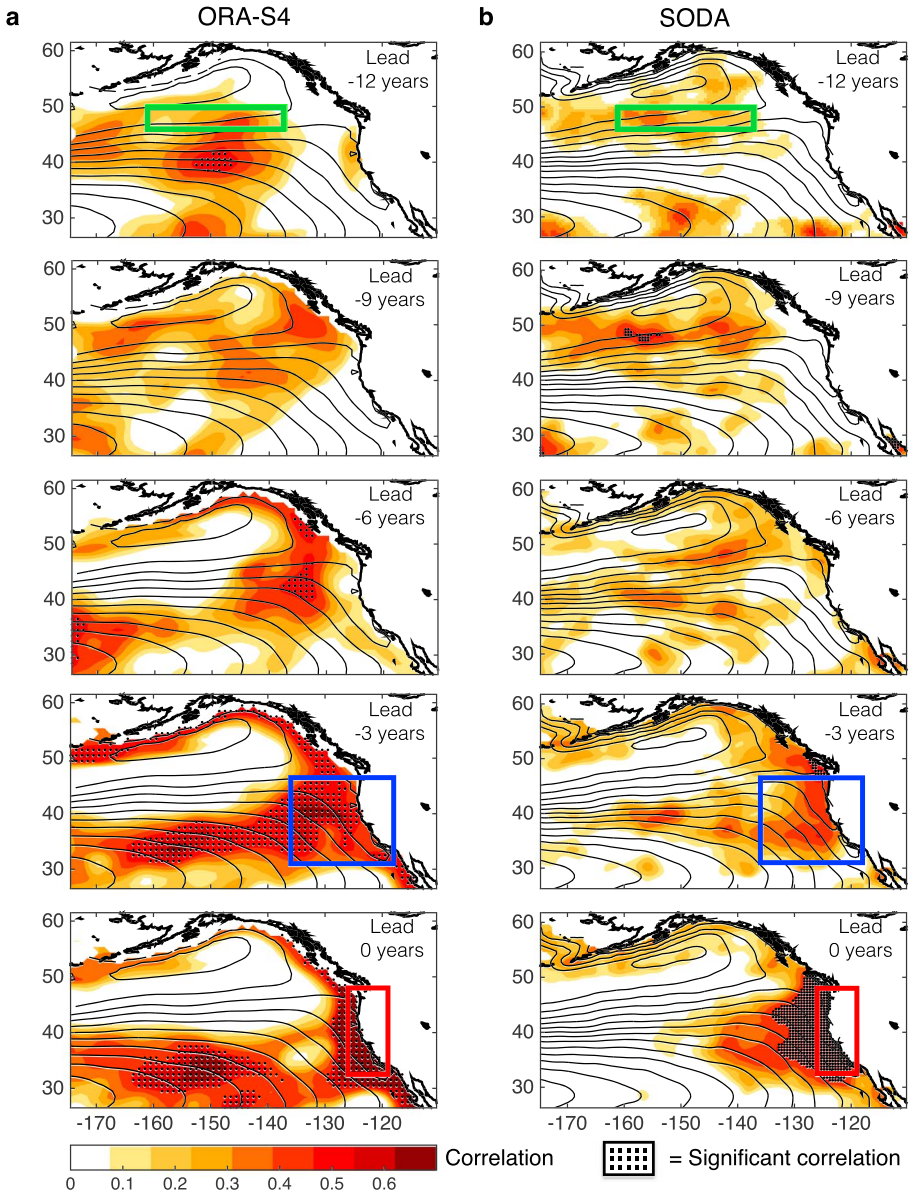

Figure 4. Lead correlation maps between the salinity anomalies on the $\sigma_\theta = 26.5$ kg m^{-3} isopycnal surface and the coastal salinity index from lead 12 to 0 years in increments of 3 years from (a) ORA-S4 and (b) SODA reanalysis products. Only positive correlations are plotted in the shading. The contours represent the mean Bernoulli's stream function along isopycnal 26.5 showing the path of the mean subsurface circulation.

These results suggest that multidecadal changes of salinity and oxygen in the CCS originate from subsurface anomalies in the North Pacific gyre rather than from the California Undercurrent. Given the decadal time scale involved in the propagation of these anomalies from the gyre, the decadal dynamics of oxygen may have inherent predictability.

5. Discussion and Implications for Decadal Predictability of Oxygen

The potential for long-term predictability of temperature, salinity, and nutrients associated with the propagation of subsurface anomalies along the North Pacific gyre has been identified in previous observational and modeling studies [*Chikamoto et al.*, 2015; *Rykaczewski and Dunne*, 2010; *Sasaki et al.*, 2010; *Taguchi and Schneider*, 2014]. Here we show that salinity anomalies, and its subsurface propagation dynamics from the North Pacific gyre into the CCS region, lead to a skillful reconstructions of the observed multidecadal

changes in CCS oxygen (Figure 3). The significant correlation ($R = 0.66$) between multidecadal fluctuations of CCS coastal salinity (i.e., a close proxy of oxygen) and salinity in the North Pacific gyre 12 year prior (Figure 3i) is suggestive of a strong relation and predicts a new decade of low-oxygen anomalies of the source waters that feed the CCS upwelling by 2020 (green time series in Figure 3i).

Although our results emphasize the role of the gyre-scale circulation in driving multidecadal subsurface tracer anomalies in the CCS, previous studies have identified the CUC as an important source of water mass anomalies in the CCS, especially in the coastal region within 100 km from the coast and in the Southern California Bight (SBC) [*Bograd et al.*, 2008, 2015; *Gay and Chereskin*, 2009; *Lynn and Simpson*, 1987; *Meinvielle and Johnson*, 2013; *Nam et al.*, 2015; *Thomson and Krassovski*, 2010]. Although our results do not exhibit a clear propagation signal from the equator, some correlation signals are displayed in the southern part of the CCS domain, near the SBC (Figures 3 and S3), which may be associated with the CUC dynamics. Furthermore, our analyses have focused on the large-scale CCS (see EOF1/PC1; Figure 2) rather than the narrow coastal boundary where CUC dynamics are important. Future studies with high-resolution ocean models will be able to diagnose the interaction dynamics between the gyre-scale and CUC signals, and their relative control on the anomalies of upwelled water masses.

Taken together, these results imply that monitoring the anomalies along the axis of the North Pacific Current may lead to decadal predictability of subsurface oxygen in the CCS and potentially of the low-frequency statistics of hypoxia along the California coast. However, the potential for decadal forecasts of oxygen in the CCS requires further testing to assess its statistical robustness. This will require the use of an ensemble approach of retrospective ocean simulations for the period of 1950–Present with a high-resolution model that adequately captures the regional circulation dynamics and scale interactions between the North Pacific gyre and the eastern boundary current system (e.g., structure and speed of the mean currents and vertical structure of temperature and salinity).

Although coarse-resolution climate model ensembles are not adequate for testing the regional predictability of oxygen in the CCS, they do provide insight on the large-scale gyre dynamics. A recent analysis of the Community Earth System Model Large Ensemble (CESM-LE) [*Kay et al.*, 2015] project from 1920 to 2100 under the greenhouse forcing scenario RCP8.5 shows a significant declining trend of subsurface oxygen on isopycnal 26.5 originating in the western North Pacific and spreading along the North Pacific Current [*Long et al.*, 2016]. This declining trend is consistent among other climate model simulations and is likely related to a reduction in oxygen solubility from ocean warming and weak ventilation from stratification and circulation changes [*Doney et al.*, 2012; *Henson et al.*, 2017; *Keeling et al.*, 2010; *Long et al.*, 2016]. According to the CESM-LE [*Long et al.*, 2016] a strong declining oxygen trend will become evident in the eastern side of the North Pacific Current (e.g., at Ocean Station Papa, 50°N, 145°W) in year ~2030, implying that CCS oxygen multidecadal variability may be exceeded by climate change-induced deoxygenation trends within the next few decades.

The decadal and predictability dynamics of oxygen explored for the California Current System may be important in similar eastern boundary upwelling systems. However, when applying these results to different ocean tracers, for example, pH (i.e., ocean acidification), it is important to consider that other dynamics associated with trend components (e.g., anthropogenic atmospheric CO_2) [*Bopp et al.*, 2013; *Hauri et al.*, 2009; *Hauri et al.*, 2013] and different memory time scales (e.g., decay) may lead to a reduction of the variance explained by the decadal propagation of anomalies from the gyre-scale circulation.

Acknowledgments
The authors are thankful to Bill Crawford for providing salinity and oxygen observations on the isopycnal layers from Ocean Station P (OSP) and Taka Ito for insightful discussions and comments. We used climatological annual average temperature, salinity, and dissolved oxygen from the World Ocean Atlas 2013 (WOA 2013) database [*Boyer et al.*, 2013] at 1° resolution, extracted from https://www.nodc.noaa.gov/OC5/woa13/woa13data.html. We also use three observational reanalysis data sets: the European Centre for Medium-Range Weather Forecasts (ECMWF) Ocean Reanalysis System 3 (ORA-S3) and 4 (ORA-S4) and the Simple Ocean Data Assimilation (SODA; version 2.1.6). Reanalysis and Argo data sets are available from the Asia-Pacific Data-Research Center (APDRC) at the University of Hawaii (http://apdrc.soest.hawaii.edu/data/data.php). This work was supported by the Pacific Ocean Eddies and Climate Study (www.pex.org) NSF-OCE 1356924 and the NSF Long Term Ecological Research California Current Ecosystem (LTER-CCE) program 3506961.

References

Balmaseda, M. A., A. Vidard, and D. L. T. Anderson (2008), The ECMWF Ocean Analysis System: ORA-S3, *Mon. Weather Rev.*, *136*(8), 3018–3034.

Balmaseda, M. A., K. Mogensen, and A. T. Weaver (2013), Evaluation of the ECMWF Ocean Reanalysis system ORAS4, *Q. J. R. Meteorol. Soc.*, *139*(674), 1132–1161.

Bograd, S. J., C. G. Castro, E. Di Lorenzo, D. M. Palacios, H. Bailey, W. Gilly, and F. P. Chavez (2008), Oxygen declines and the shoaling of the hypoxic boundary in the California Current, *Geophys. Res. Lett.*, *35*, L12607, doi:10.1029/2008GL034185.

Bograd, S. J., M. Pozo Buil, E. Di Lorenzo, C. G. Castro, I. D. Schroeder, R. Goericke, C. R. Anderson, C. Benitez-Nelson, and F. A. Whitney (2015), Changes in source waters to the Southern California Bight, *Deep Sea Res., Part II*, *112*, 42–52, doi:10.1016/j.dsr2.2014.04.009.

Bopp, L., et al. (2013), Multiple stressors of ocean ecosystems in the 21st century: Projections with CMIP5 models, *Biogeosciences*, *10*(10), 6225–6245, doi:10.5194/bg-10-6225-2013.

Boyer, T. P., et al. (2013), World Ocean Database 2013, NOAA Atlas NESDIS 72, edited by S. Levitus, A. Mishonov, Technical Ed., 209 pp., Silver Spring, Md, doi:10.7289/V5NZ85MT.

Carton, J. A., and B. S. Giese (2008), A reanalysis of ocean climate using Simple Ocean Data Assimilation (SODA), *Mon. Weather Rev.*, *136*(8), 2999–3017, doi:10.1175/2007mwr1978.1.
Chan, F., J. A. Barth, J. Lubchenco, A. Kirincich, H. Weeks, W. T. Peterson, and B. A. Menge (2008), Emergence of anoxia in the California Current large marine ecosystem, *Science*, *319*(5865), 920–920.
Checkley, D. M., and J. A. Barth (2009), Patterns and processes in the California Current System, *Prog. Oceanogr.*, *83*(1–4), 49–64, doi:10.1016/j.pocean.2009.07.028.
Chhak, K. C., E. Di Lorenzo, N. Schneider, and P. F. Cummins (2009), Forcing of low-frequency ocean variability in the Northeast Pacific*, *J. Clim.*, *22*(5), 1255–1276, doi:10.1175/2008jcli2639.1.
Chikamoto, M. O., A. Timmermann, Y. Chikamoto, H. Tokinaga, and N. Harada (2015), Mechanisms and predictability of multiyear ecosystem variability in the North Pacific, *Global Biogeochem. Cycles*, *29*, 2001–2019, doi:10.1002/2015GB005096.
Chu, P. C., R. F. Li, and X. B. You (2002), Northwest Pacific subtropical countercurrent on isopycnal surface in summer, *Geophys. Res. Lett.*, *29*(17), 1842, doi:10.1029/2002GL014831.
Connolly, T. P., B. M. Hickey, S. L. Geier, and W. P. Cochlan (2010), Processes influencing seasonal hypoxia in the northern California Current System, *J. Geophys. Res.*, *115*, C03021, doi:10.1029/2009JC005283.
Crawford, W. R., and M. A. Pena (2016), Decadal trends in oxygen concentration in subsurface waters of the Northeast Pacific Ocean, *Atmos. Ocean*, *54*(2), 171–192, doi:10.1080/07055900.2016.1158145.
Deutsch, C., S. Emerson, and L. Thompson (2006), Physical-biological interactions in North Pacific oxygen variability, *J. Geophys. Res.*, *111*, C09S90, doi:10.1029/2005JC003179.
Deutsch, C., H. Brix, T. Ito, H. Frenzel, and L. Thompson (2011), Climate-forced variability of ocean hypoxia, *Science*, *333*(6040), 336–339, doi:10.1126/science.1202422.
Di Lorenzo, E., and M. D. Ohman (2013), A double-integration hypothesis to explain ocean ecosystem response to climate forcing, *Proc. Natl. Acad. Sci. U.S.A.*, *110*(7), 2496–2499, doi:10.1073/pnas.1218022110.
Di Lorenzo, E., et al. (2008), North Pacific Gyre Oscillation links ocean climate and ecosystem change, *Geophys. Res. Lett.*, *35*, L08607, doi:10.1029/2007GL032838.
Diaz, R. J., and R. Rosenberg (2008), Spreading dead zones and consequences for marine ecosystems, *Science*, *321*(5891), 926–929, doi:10.1126/science.1156401.
Doney, S. C., et al. (2012), Climate change impacts on marine ecosystems, *Ann. Rev. Mar. Sci.*, *4*(1), 11–37, doi:10.1146/annurev-marine-041911-111611.
Garcia, H. E., and L. I. Gordon (1992), Oxygen solubility in seawater—Better fitting equations, *Limnol. Oceanogr.*, *37*(6), 1307–1312.
Gay, P. S., and T. K. Chereskin (2009), Mean structure and seasonal variability of the poleward undercurrent off southern California, *J. Geophys. Res.*, *114*, C02007, doi:10.1029/2008JC004886.
Grantham, B. A., F. Chan, K. J. Nielsen, D. Fox, J. A. Barth, A. Huyer, J. Lubchenco, and B. A. Menge (2004), Upwelling-driven nearshore hypoxia signals ecosystem and oceanographic changes in the northeast Pacific, *Nature*, *429*, 749–754.
Hauri, C., N. Gruber, Z. Lachkar, and G. K. Plattner (2009), Accelerated acidification in eastern boundary current systems, *Geochim. Cosmochim. Acta*, *73*(13), A503–A503.
Hauri, C., N. Gruber, M. Vogt, S. C. Doney, R. A. Feely, Z. Lachkar, A. Leinweber, A. M. P. McDonnell, M. Munnich, and G. K. Plattner (2013), Spatiotemporal variability and long-term trends of ocean acidification in the California Current System, *Biogeosciences*, *10*(1), 193–216, doi:10.5194/bg-10-193-2013.
Henson, S. A., C. Beaulieu, T. Ilyina, J. G. John, M. Long, R. Seferian, J. Tjiputra, and J. L. Sarmiento (2017), Rapid emergence of climate change in environmental drivers of marine ecosystems, *Nat. Commun.*, *8*, 14682, doi:10.1038/ncomms14682.
Hickey, B. M. (1979), The California Current System—Hypotheses and facts, *Prog. Oceanogr.*, *8*(4), 191–279, doi:10.1016/0079-6611(79)90002-8.
Ito, T., and C. Deutsch (2010), A conceptual model for the temporal spectrum of oceanic oxygen variability, *Geophys. Res. Lett.*, *37*, L03601, doi:10.1029/2009GL041595.
Kay, J. E., et al. (2015), The Community Earth System Model (CESM) Large Ensemble project a Community resource for studying climate change in the presence of internal climate variability, *Bull. Am. Meteorol. Soc.*, *96*(8), 1333–1349, doi:10.1175/Bams-D-13-00255.1.
Keeling, R. F., A. Kortzinger, and N. Gruber (2010), Ocean deoxygenation in a warming world, *Annu. Rev. Mar. Sci.*, *2*, 199–229, doi:10.1146/annurev.marine.010908.163855.
Kilpatrick, T., N. Schneider, and E. Di Lorenzo (2011), Generation of low-frequency spiciness variability in the thermocline, *J. Phys. Oceanogr.*, *41*(2), 365–377, doi:10.1175/2010jpo4443.1.
Koslow, J. A., R. Goericke, A. Lara-Lopez, and W. Watson (2011), Impact of declining intermediate-water oxygen on deepwater fishes in the California Current, *Mar. Ecol. Prog. Ser.*, *436*, 207–218, doi:10.3354/Meps09270.
Long, M. C., C. Deutsch, and T. Ito (2016), Finding forced trends in oceanic oxygen, *Global Biogeochem. Cycles*, *30*, 381–397, doi:10.1002/2015GB005310.
Lynn, R. J., and J. J. Simpson (1987), The California Current System—The seasonal variability of its physical characteristics, *J. Geophys. Res.*, *92*, 12,947–12,966, doi:10.1029/JC092iC12p12947.
Mantua, N. J., S. R. Hare, Y. Zhang, J. M. Wallace, and R. C. Francis (1997), A Pacific interdecadal climate oscillation with impacts on salmon production, *Bull. Am. Meteorol. Soc.*, *78*(6), 1069–1079, doi:10.1175/1520-0477(1997)078<1069:Apicow>2.0.Co;2.
McClatchie, S., R. Goericke, R. Cosgrove, G. Auad, and R. Vetter (2010), Oxygen in the Southern California Bight: Multidecadal trends and implications for demersal fisheries, *Geophys. Res. Lett.*, *37*, L19602, doi:10.1029/2010GL044497.
Meinvielle, M., and G. C. Johnson (2013), Decadal water-property trends in the California Undercurrent, with implications for ocean acidification, *J. Geophys. Res. Oceans*, *118*, 6687–6703, doi:10.1002/2013JC009299.
Nam, S., Y. Takeshita, C. A. Frieder, T. Martz, and J. Ballard (2015), Seasonal advection of Pacific equatorial water alters oxygen and pH in the Southern California Bight, *J. Geophys. Res. Oceans*, *120*, 5387–5399, doi:10.1002/2015JC010859.
Peterson, J. O., C. A. Morgan, W. T. Peterson, and E. Di Lorenzo (2013), Seasonal and interannual variation in the extent of hypoxia in the northern California Current from 1998–2012, *Limnol. Oceanogr.*, *58*(6), 2279–2292, doi:10.4319/lo.2013.58.6.2279.
Pierce, S. D., J. A. Barth, R. K. Shearman, and A. Y. Erofeev (2012), Declining oxygen in the northeast Pacific, *J. Phys. Oceanogr.*, *42*(3), 495–501, doi:10.1175/Jpo-D-11-0170.1.
Pozo Buil, M., and E. Di Lorenzo (2015), Decadal changes in Gulf of Alaska upwelling source waters, *Geophys. Res. Lett.*, *42*, 1488–1495, doi:10.1002/2015GL063191.
Rabalais, N. N., R. J. Diaz, L. A. Levin, R. E. Turner, D. Gilbert, and J. Zhang (2010), Dynamics and distribution of natural and human-caused hypoxia, *Biogeosciences*, *7*(2), 585–619.

Rykaczewski, R. R., and J. P. Dunne (2010), Enhanced nutrient supply to the California current ecosystem with global warming and increased stratification in an earth system model, *Geophys. Res. Lett.*, *37*, L21606, doi:10.1029/2010GL045019.
Sasaki, Y. N., N. Schneider, N. Maximenko, and K. Lebedev (2010), Observational evidence for propagation of decadal spiciness anomalies in the North Pacific, *Geophys. Res. Lett.*, *37*, L07708, doi:10.1029/2010GL042716.
Stramma, L., S. Schmidtko, L. A. Levin, and G. C. Johnson (2010), Ocean oxygen minima expansions and their biological impacts, *Deep Sea Res., I*, *57*, 587–595, doi:10.1016/j.dsr.2010.01.005.
Taguchi, B., and N. Schneider (2014), Origin of decadal-scale, eastward-propagating heat content anomalies in the North Pacific, *J. Clim.*, *27*(20), 7568–7586, doi:10.1175/Jcli-D-13-00102.1.
Thomson, R. E., and M. V. Krassovski (2010), Poleward reach of the California Undercurrent extension, *J. Geophys. Res.*, *115*, C09027, doi:10.1029/2010JC006280.
Unesco (1983), Algorithms for computation of fundamental properties of seawater, 1983, Unesco Tech. Pap. Mar. Sci., No. 44, 53 pp.
Veronis, G. (1972), Properties of seawater defined by temperature, salinity, and pressure, *J. Mar. Res.*, *30*(2), 227.
Whitney, F. A., H. J. Freeland, and M. Robert (2007), Persistently declining oxygen levels in the interior waters of the eastern subarctic Pacific, *Prog. Oceanogr.*, *75*(2), 179–199, doi:10.1016/j.pocean.2007.08.007.
Wyrtki, K. (1962), The oxygen minima in relation to ocean circulation, *Deep Sea Res.*, *9*(1), 11–23, doi:10.1016/0011-7471(62)90243-7.